32p.

# FINE STRUCTURE OF THE ABSORPTION CROSS-SECTION OF GASES IN THE ULTRAVIOLET AND AN ANALYSIS OF THE RAY SYSTEM OF THE LUNAR CRATER TYCHO

Principal Investigator: William A. Rense

UNIVERSITY OF COLORADO
Laboratory for Atmospheric and Space Physics
Boulder, Colorado

May, 1964



SCIENTIFIC REPORT NO. 3
N.A.S.A. Contract No. NASr-86
September, 1963 - April, 1964



Prepared by
Martin Sedlacek

for
NATIONAL AERONAUTICS AND SPACE ADMINISTRATION
WASHINGTON 25, D. C.

# PREFACE

In this report two problems are considered; one involving the design of an instrument for an experiment directed toward measuring the energy spectrum of electrons, and the other a theoretical investigation of the Tycho ray system on the moon. In each case the work was carried out by Dr. Martin Sedlacek, NASA International University Fellow from the University of Vienna, who was associated with the Laboratory for Atmospheric and Space Research from September 1963 to June 1964.

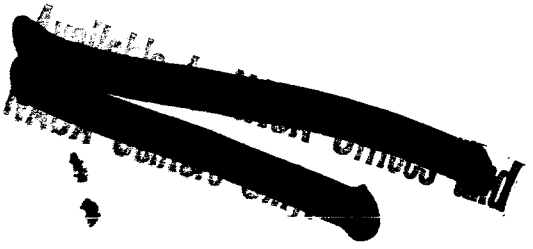

# CHAPTER 1

## FINE STRUCTURE OF THE ABSORPTION CROSS-SECTION OF GASES IN THE ULTRAVIOLET

### I. Introduction

The absorption of photons in a gas will result in different processes [1]:

a) Ionization and excitation of the molecular ion to a vibrational or rotational state

b) Dissociative ionization

c) Extraction of more firmly bounded electrons, provided the wavelength is short enough

The experimental material on the total absorption and ionization cross-sections in the ultra-violet already covers the wavelength range down to 150 Å [2,3] and a wide variety of gases. The observational data on the "fine-structure" of the absorption, i.e. which fraction of the total cross-section is referred to one of the processes mentioned above, are quite incomplete. Therefore the energy-distribution of the photoelectrons produced by the absorption process is unknown. Weissler and co-workers [4] analyzed the absorption process by measuring the relative numbers of atomic and molecular ions by means of a mass-spectrometer and by interpreting changes in the ion-current intensities as the appearance of ions in higher excited states. Experiments on secondary electrons produced by molecule-ion and molecule-electron collision have been made by several investigators [5,6,7] . The only work on the energy of photo-electrons in gases seems to be the article of Viselov [1] , dealing with organic vapors and wavelengths down to about 1080 Å.

The experiment described in this proposal is designed to measure the energy-distribution of the photoelectrons, thus revealing the fine-structure of the absorption process. The knowledge of both quantities (electron-energy and fine-structure) is of major interest as a basis of calculations in theories concerning electrical and optical phenomena in the high atmosphere.

II. The Experimental Apparatus

The instrument will consist of three main parts:

1) The vacuum-monochromator and the lightsource
2) Ionization-chamber and electron-spectrometer
3) Detector and counter

1) Light source and monochromator may be one of several commercial types available. They could be adapted to fit the requirements of the experiment. The other parts need a complete new design, described in more detail in the following sections.

2) The electron-spectrometer:

a) Basic requirements: In order to avoid distortion of the original electron-energy-spectrum, care is required in mininizing the fraction of photoelectrons scattered or absorbed by the gas which fills the spectrometer. Kollath[8] reported scattering and absorption cross-sections $\sigma$ for many monatomic and diatomic gases ranging from 5 to 140 $cm^2/cm^3$ (at 0°C, 1 mm Hg, and an electron-energy up to 36 eV). Assuming a path-length of 10 cm and a $\sigma$ =100 $cm^2/cm^3$ the pressure in the spectrometer-detector-system should not exceed $10^{-5}$ mm Hg, thus reducing the scattered fraction of the electron-beam to 1% or less.

As low-energy-electrons are strongly influenced even by weak magnetic fields, shielding or compensation of the earth-field and the random laboratory fields is required. Due to its simplicity shielding by mu-metal tubes is superior to the compensation, which needs a control system continuously monitoring and compensating the field variations.

b) The parallel-plate electrostatic spectrometer and its basic equations:

As an instrument for electron-spectroscopy at low energies up to a few hundred eV an electrostatic analyzer is superior to a magnetic one, especially in avoiding the difficulties involved in the production of highly uniform magnetic fields by coils. The departure from perfect focusing is of the same order of magnitude in both cases. For the proposed experiment

a parallel-plate-analyzer [9] could be used. The structure is simple, very similar to that of a two-plate condensor. The following will give the theory of the instrument in more detail, because of the lack of a complete focusing-error analysis in the literature.

The range s of an electron (energy $E_p = eU_p$) in a uniform opposing electrostatic field is given by

$$(1) \qquad s = \frac{2\nu_o^2 \sin\alpha \cos\alpha}{b} \qquad \text{(see fig. 1a)}$$

where $\alpha$ is the inclination of the electron-beam to the xy-plane at the entrance-slit. The quantities b and $\nu_o^2$ are defined by the relations

$$b = \frac{e}{m} \cdot F = \frac{e}{m} \frac{U_c}{D} \quad \text{and} \quad \nu_o^2 = \frac{2e}{m} \cdot U_p$$

giving (2) $$s = 4 \frac{U_p}{U_c} \cdot D \sin\alpha \cos\alpha$$

The maximum range $s_{max}$ is due to an angle $\alpha$ of 45°, resulting in the basic equations of the analyzer:

$$(I) \quad s_{45} = s_{max} = \frac{2U_p}{U_c} \cdot D$$

$$(Ia) \quad U_p = \frac{s_{max}}{2D} \cdot U_c$$

As D (the plate-distance) and $s_{max}$ (distance entrance-to exit-slit) are given by the spectrometer geometry the energy spectrum of the incident electron -beam is scanned by variation of $U_c$.

c) Energy resolution and slit dimensions: A beam of monoenergetic electrons passing the entrance slit will result in an "image" of the slit at the distance s, the width of the image depending on the deviation $\varphi$ from the mean inclination $\alpha = 45°$, on the maximum value of $\psi$ (see fig. 1b, 2a) and on the dimensions of the entrance slit itself.

$$(3)\quad s_\psi = s_{\psi=o}\cdot\cos\psi = {}_{\psi=o}\cdot\left(1-\frac{\psi^2}{2}\right),\ \psi \ll 1 \quad \text{(Fig. 1b)}$$

$$(4)\quad s_{45\pm\varphi} = s_{max}\cdot\sin(90\pm 2\varphi) = s_{max}\,(1-2\varphi^2) \qquad \varphi \ll 1$$

Combination of the equations (3) and (4) yields:

$$\text{(II)}\quad s_{\psi,\varphi} = s_{max}\cdot\left(1-2\varphi^2-\frac{\psi^2}{2}\right)$$

If one considers the width b of the entrance-slit, the total focusing error s is given by:

$$\text{(III)}\quad \Delta s = s_{max} - s_{\psi,\varphi} + b = s_{max}\left(2\varphi^2+\frac{\psi^2}{2}\right) + b \quad \text{(Fig. 2b)}$$

To electronbeams with energies $E_1 > E_2$ are completely separated by the spectrometer if their s-values fulfill the equation (see Fig. 3):

$$(5)\quad {}_2s_{max} + b = {}_1s_{max}\left(1-2\varphi^2-\frac{\psi^2}{2}\right)$$

or $$(5a)\quad {}_2s_{max} = {}_1s_{max} - \triangle\,{}_1s$$

As E is proportional to s (equation Ia), the energy resolution is given by

$$\text{(IV)}\quad \eta = \frac{\triangle E}{E} = \frac{\Delta s}{s} = 2\varphi^2_{max} + \frac{\psi^2 max}{2} + \frac{b}{s_{max}}$$

The angles $\varphi_{max}$ and $\psi_{max}$ are defined by the geometry of the system (Fig. 2b, 2c)

$$(6a)\quad \tan\varphi_{max} = \varphi = \frac{b/\sqrt{2}}{\sqrt{2}a_n \pm \frac{b}{2\sqrt{2}}} = \frac{b}{2a_n} \qquad b \ll 4a_n$$

$$(6b)\quad a_n\sqrt{2} = a_\ell$$

$$(7)\quad \tan \psi_{max} = \psi = \frac{\ell}{a_\ell + 1.1477 s}$$

if the slits A, B, and B' are considered to be equal in length $\ell$ (Fig. 2a). The index "max" is omitted in the following section.

d) Spectrometer-dimensions (s = 75 mm, $\eta$ = 2%); If s and $\eta$ are given, all other dimensions of the spectrometer follow from the equations derived in the previous chapter. Assuming s = 75 mm and $\eta$ = 2% equation (IV) yields:

$$2 \cdot 10^{-2} = 2\varphi^2 + \frac{\psi^2}{2} + \frac{b}{75}$$

Values for b, $\varphi$ and $\psi$ are found to be

$$b = 0.50 \text{ mm}, \quad \varphi = 0.057735. \quad \psi = 0.11547$$

if one makes all three contributions to $\eta$ equal. The transmissivity

$$T = \varphi\psi / 2\pi = 1.061 \cdot 10^{-3}$$

According to equations (6a, 6b)

$$a_n = 4.33 \text{mm}. \quad a_\ell = 6.124 \text{ mm}.$$

The value of $\ell$ = 10.65 mm is derived by using $a_\ell$ and s in equation (7). The following table summarizes the results:

$$s = 75 \text{ mm}, \quad \eta = 2\%$$
$$\Delta s = 1.5 \text{ mm}, \quad D \geq \frac{s}{4} = 18.75 \text{ mm}$$
$$b = 0.50 \text{ mm}, \quad \varphi = 0.05774, \quad \psi = 0.11547, \quad T = 1.06.10^{-3}$$
$$d = b/\sqrt{2} = 0.354 \text{ mm}, \quad a_n = 4.33 \text{ mm}, \quad a_\ell = 6.124 \text{ mm}$$
$$\ell = 10.65 \text{ mm}$$
$$\overline{OB'}_1 = 73.75 \text{ mm}, \quad \overline{OB'}_2 = 75.25 \text{ mm} \quad \text{(see Fig. 2b)}$$

Figures 4a, b, c show a 1:1 cross-section of the spectrometer and details of the slit system A, B, and B'. The voltage $U_c$ between the ground-plate P and the fine mesh G provides the opposing analyzer field. D is arbitrarily chosen to be 25 mm; the voltage $U_c$ for a particle energy $eU_p$ follows from equation (Ia). Electrons exceeding a certain energy will pass the mesh G and will be trapped at T. This precaution should help to minimize electron

backscattering and secondary electron emission at G. Backscattered electrons, now accelerated towards the exit-slit, could obscure the original energy spectrum. The sawtooth shape of the slit system AB (defining $\varphi$) should prevent scattered electrons from entering the spectrometer. Machining the system from one solid block of material avoids the aligning of single slits and reduces contact potentials. The filament F in figure 4a provides a means for testing the analyzing and detecting system.

If the area of ionization is enclosed by a chamber (1...5 in Fig. 4a) the gasflow to the spectrometer has to pass the slit system AB with a conductivity of

$$(8)\quad L = 3.64\ \frac{d \cdot f}{0.19 \cdot a_f \frac{(2d + 2f)}{d \cdot f} + 1}\sqrt{\frac{T}{M}} \quad \text{(liters/sec)}$$

(all dimensions in cm [10]). For $N_2$, a temperature of 300°K and the calculated slit dimensions, L follows to be $5.8 \times 10^{-2}$ liters/sec. The amount Q of $N_2$ flowing through the slit may be calculated from the equation:

$$(8a)\quad L(p_1 - p_2) = Q(\text{mmHg liters/sec})\ [11]$$

For $p_1 = 10^{-5}$ mmHg and $p_2 \ll p_1$ (maximum gas flow Q) Q is equal to $5.8 \times 10^{-7}$ mmHg liters/sec for $N_2$. A pump with a speed of a few liters per second at a pressure of $10^{-6}$ mmHg should be able to lower the pressure $p_2$ to one fifth or one tenth of $p_1$, thus reducing the fraction of photoelectrons scattered by the gas in the spectrometer to a negligible value.

3) The detecting system

a) Electron flux through the exit slit B':

The energy-flux through the exit slit of a grazing incidence monochromator varies widely with the wavelength of the light, but for typical instruments now in use such as at LASP, it can be expected to be at least 1 erg/sec in the range 300 to 1200 Å (slit-dimensions 0.8 x 10mm) [12]. Crossing the exit slit of the monochromator with the system AB of the electron spectrometer avoids errors due to misalignments of both systems,

but reduces the useful photon-flux in the region I (Fig. 4a) seen by AB to about $5 \times 10^{-2}$ erg/sec or $0.76 \times 10^{9}$ photons/sec at $\lambda = 300$ Å. At this wavelength for $N_2$ Curtis [2] measured an absorption coefficient $K = 125\ cm^{-1}$ (referred to normal temperature and pressure). At $p = 10^{-5}$ mmHg the above mentioned photon flux therefore leads to a production of about $1.33 \times 10^{3}$ electrons per second along a pathlength of $\ell = 1.065$ cm. The number of electrons passing the slit B' of the electron spectrometer is proportional to $T = 10^{-3}$ and $\eta = 2 \times 10^{-2}$ (assuming the electrons equally distributed over the whole energy-range under consideration) ; hence one can expect a mean value of 1.6 electrons/minute passing B'.

b) The detector

The number of electrons calculated in the previous paragraph gives a lower limit of the flux as both photons per erg and absorption coefficient increase with increasing wavelength; nevertheless one has to use single pulse counting with a low background detector. A major problem is the low energy of the photoelectrons. The use of a Geiger-Muller counter calls for accelerations of the electrons up to 25 keV, even if the window is only a few thousand Å thick. Corona discharges and fluctuations in the high-voltage supply could give rise to spurious counts introducing errors in the result. An open electron multiplier with low work function dynode structure has too much thermal noise, obscuring the few counts due to photoelectrons. The variation of the total gain with gas pressure and the gas-contamination of the dynodes makes the application of a pulse-height discriminator for background reduction difficult and the result uncertain.

According to Hinteregger [13] a magnetic resistance strip electron multiplier (Bendix-type) with a continuous high work function coating both on dynode and field strip has a background rate of only 6 counts per minute, allowing the detection of a few counts per minute over background in a reasonable short time. The electrons need acceleration only up to an energy of 800 to 1000 eV for penetration of the opposing field in the multiplier. Thus the magnetic resistance strip multiplier seems to be the detector best applicable to the problem of counting low energy electrons. Nevertheless the first step in building the apparatus should be the testing of the background and the efficiency of the detector in use.

Figure Captions

Fig. 1a & 1b: Basic analyzer-geometry (Eq. 1).

Fig. 2a: Geometrical definition of $\psi_{max}$ (A, B, B' equal in length).

Fig. 2b: Distances in the entrance-exit slit system, as given by s, b, $\varphi$ and $\psi$ (index "max" omitted).

Fig. 2c: Geometry defining the deviation $\pm \varphi_{max}$ from the mean inclination $\alpha = 45°$.

Fig. 3: Spatial separation of two electron beams with energies $E_1 > E_2$.

Fig. 4a: Cross-section of the electron spectrometer. $U_c$ between G and P provides the opposing electrostatic separator field. 1....5 Ionization chamber, I = area of ionization.

Fig. 4b and 4c: Details of entrance and exit slit systems. (Slits bevelled according to the direction of the electron flux).

Fig. 5: Position of the magnetic resistance strip multiplier (MRSM) opposit the exit slit B'. (No multiplier voltages are given because they depend upon the MRSM in use). The electrons passing B' with a mean inclination of 45° are accelerated by the uniform electrostatic field between H and the field strip ($U_a$ = accel. voltage) in order to penetrate the opposing field in the MRSM.

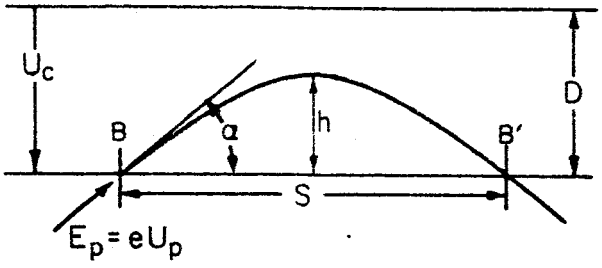


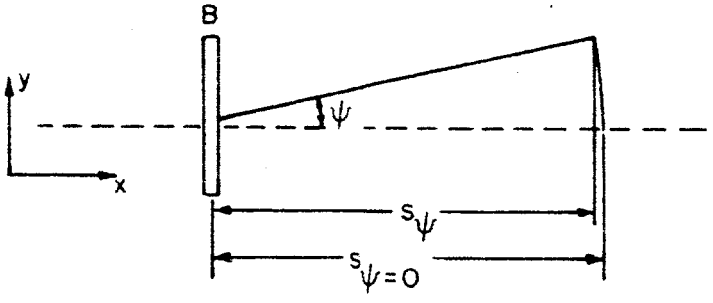


Fig. 1a and Fig. 1b

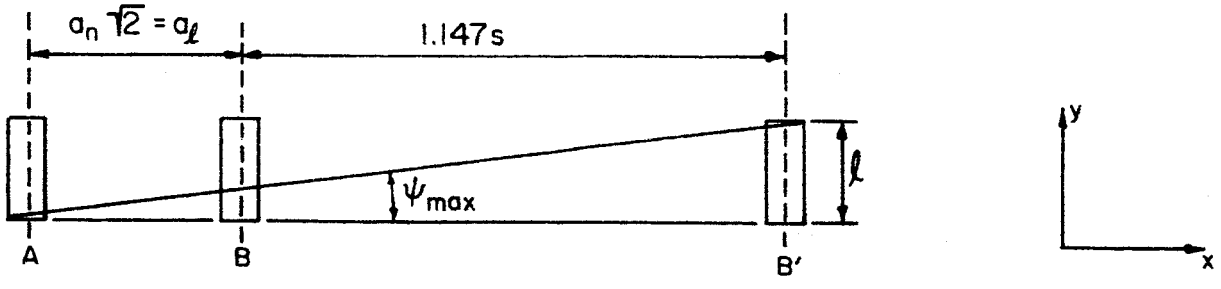


Fig. 2a

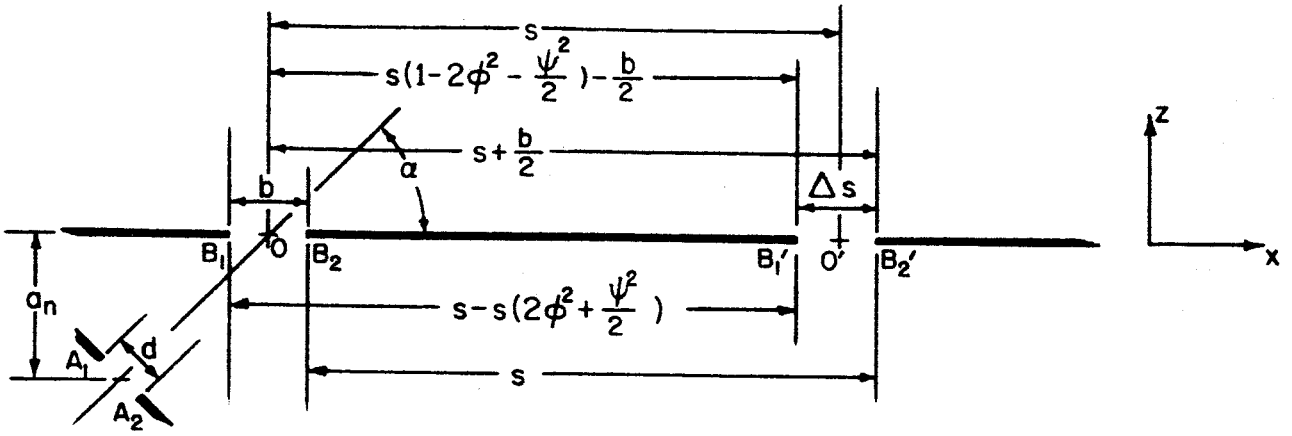
s
$s(1-2\phi^2-\frac{\psi^2}{2})-\frac{b}{2}$
$s+\frac{b}{2}$
α
b
Δs
z
x
$B_1$
O
$B_2$
$B_1'$
O'
$B_2'$
$a_n$
$s-s(2\phi^2+\frac{\psi^2}{2})$
d
$A_1$
$A_2$
s

Fig. 2b

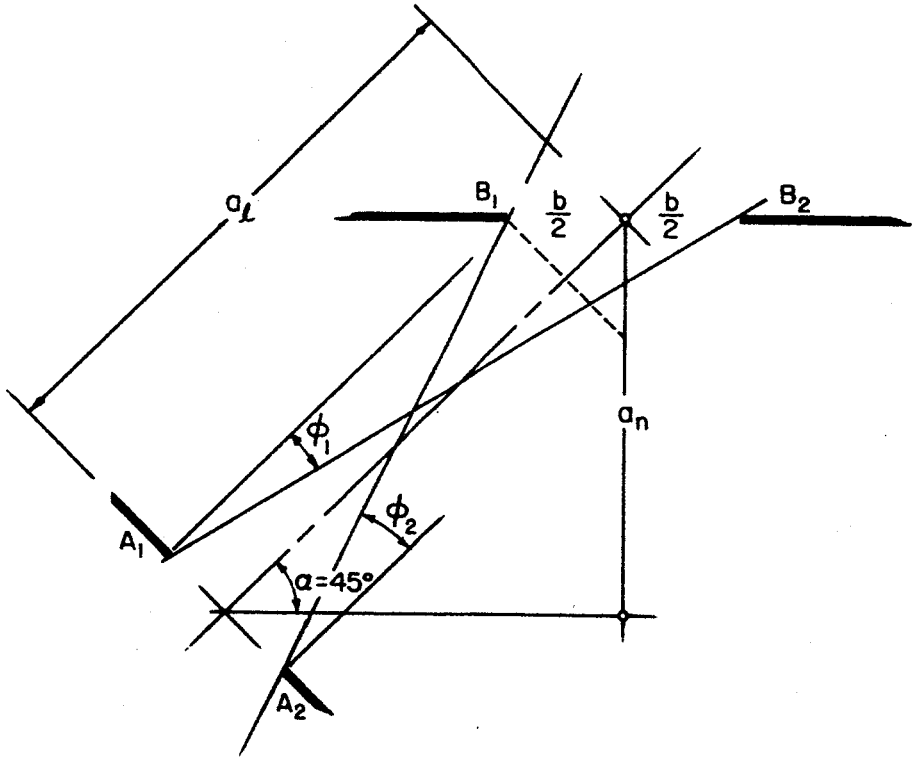
$a_l$
$B_1$
$\frac{b}{2}$
$\frac{b}{2}$
$B_2$
$a_n$
$\phi_1$
$\phi_2$
$A_1$
α=45°
$A_2$

Fig. 2c

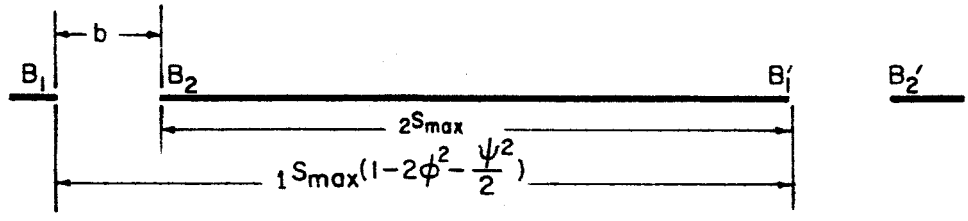
b
B1
B2
B1'
B2'
2Smax
1Smax(1-2φ²-ψ²/2)

Fig. 3

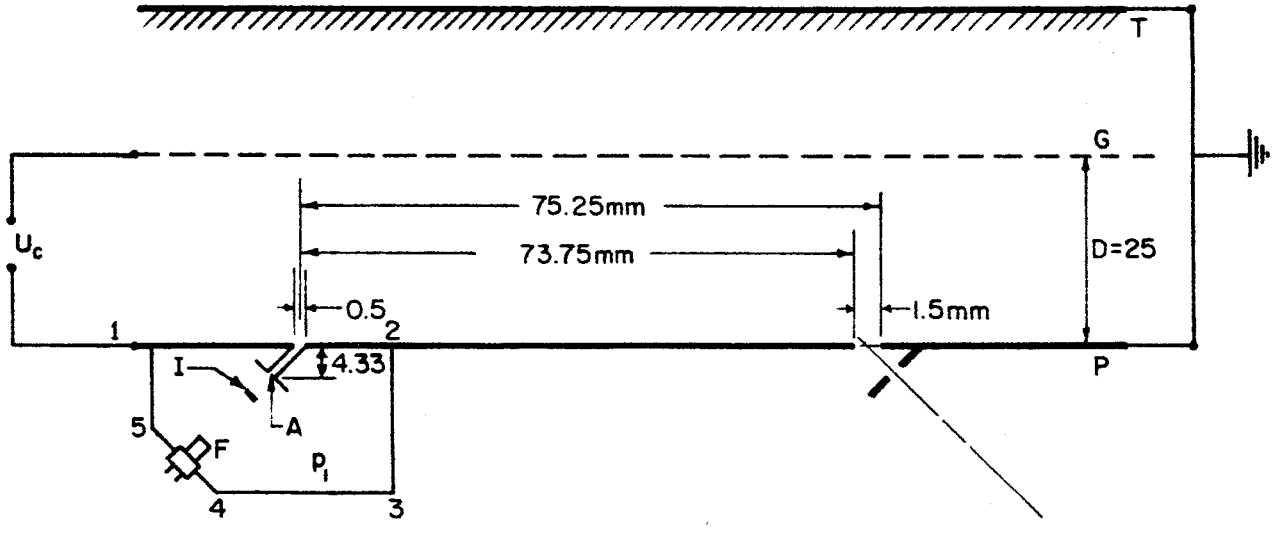
T
G
Uc
75.25mm
73.75mm
D=25
0.5
1.5mm
1
2
4.33
I
A
5
F
P1
4
3
P

Fig. 4a

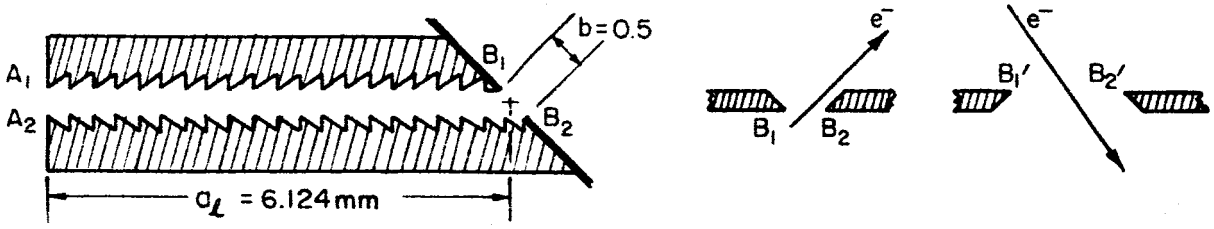


Fig. 4b and Fig. 4c

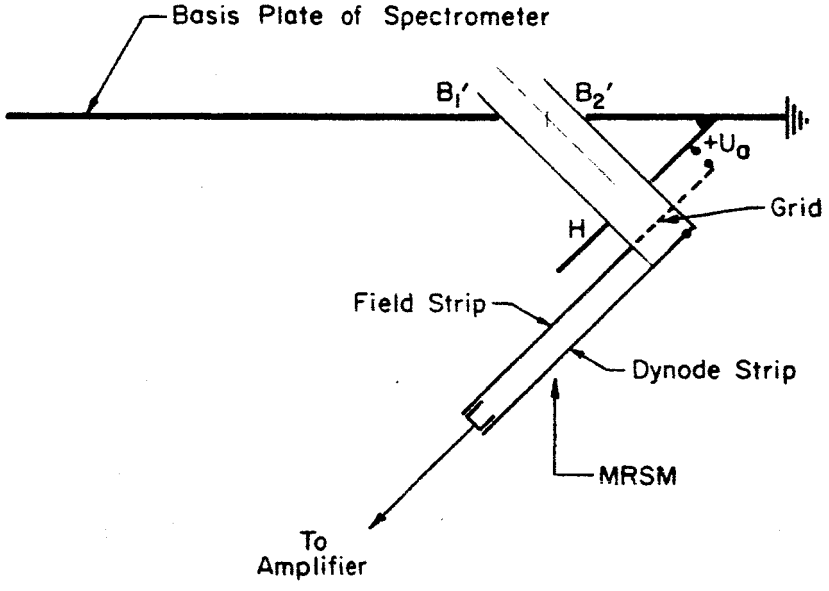


Fig. 5

References

1. Viselov F. I., Kurbatov B. L., Terenin A. N.: Sovj. Phys. Dokl. Vol. 6, No. 6, 490 - 493 (March 1961).

2. Curtis J. P.: Phys. Rev. Vol. 94, No. 4, 908 - 910 (May 1954).

3. Weissler G. L.: Handbuch der Physik (S. Flügge Ed.) Vol. 21, Springer-Verlag, Berlin (1956).

4. Weissler G. L., Samson J. A. R., Ogava M., Cook G. R.: JOSA Vol. 49, No. 4, 338 - 349 (April 1959).

5. Berry H. W.: Phys. Rev. Vol. 121, No. 6, 1714 - 1719 (March 1961).

6. Moe D. E., Petsch O. H.: Phys. Rev. Vol. 110, No. 6. 1358 - 1361 (June 1958).

7. Moe D. E, Petsch O. H.: Phys. Rev. Vol. 115, No. 2, 349 - 350 (July 1959).

8. Kollath R.: Handbuch der Physik (S. Flügge Ed.) Vol. 34, 1 - 52, Springer-Verlag, Berlin (1958).

9. Yarnold G. D., Bolton H. C.: Journ. Sci. Instr. Vol. 26, No. 2, 38 - 40 (Feb. 1949).

10. von Ardenne M.: Tabellen der Elektronenphysik, Vol. II, 677, Deutscher Verlag der Wissenschaften, Berlin (1956).

11. Dushman S.: Scientific Foundations of Vacuum Technique, 91 J. Wiley and Sons, New York (1949).

12. Bruner E. C.: personal communication

13. Hinteregger H. E., Heroux L.: Rev. Sci. Instr. Vol. 31, No. 3, 280 - 286 (March 1960).

# CHAPTER 2

## AN ANALYSIS OF THE RAY SYSTEM OF THE LUNAR CRATER TYCHO

### I. Introduction

The ray systems on the moon, the mechanism of their formation and the possibility of studying them as a key to the moon's period of rotation at the time when the material has been deposited, are widely discussed in the astronomical literature. (For a summary of the problem see Fielder 1961 and Wright et al. 1963). However, the Giamboni publication (1959) seems to be the only one to deal with an extensive mathematical analysis of the most prominent ray systems, those of Tycho and Copernicus. As a result of his analysis the author finds a period of rotation from 0.5 to 6.8 days at the time of ray-formation and suggests that the position of the poles did not change too much since then.

The following paper is based on the very long rays of the Tycho system and the conclusions are entirely different from the results given in the publication mentioned above.

### II. Lunar Ballistics

Particles ejected with identical azimuths--i.e.orbits in the same vertical plane--by volcanic action or meteorite impact on a non-rotating spherical body are deposited along the arc of a great circle. Rotation of the sphere causes changes in the pattern of deposition, the changes depending on the time of flight of the material, the period of revolution, and the location of the source with respect to the axis of rotation.

The particle orbit o (Fig. 1) is stable in space and, at the moment of ejection, above the great circle c with an azimuth $\varphi_s$. During the time of flight $t_f$, point source S and great circle c move into the positions $S_t$ and $c_t$. Thus the particle falls at P' instead of P. The deviation $\Delta\alpha = \frac{2\pi}{\tau} t_f$ is always measured along a parallel circle p through P. If source and rays are entirely on one half-sphere, the deposit-pattern is "central" symmetric, the curvature of the rays is either left- or right-handed, provided that the ejection angles and velocities are similar for all rays, as the curvature

depends upon the angle of ejection, the ratio of the velocities in the particle beam to the velocity $v_T$ of the source, etc. A source close to or on the equator gives rise to a "mirror" symmetric pattern, in this case the curvature is left-handed on one side, right-handed on the other side of the equator.

The initial velocity $\vec{v}_s$ in the space stable orbit o is the sum of the velocity $\vec{v}_o$ relative to the rotating coordinate-system and the tow-speed $\vec{v}_T = \omega R \cos B$ due to the rotation of the moon.

Using a coordinate-system (Fig. 2) with the origin in S, the x-axis parallel to $\vec{v}_T$, the y-axis normal to $\vec{v}_T$ and in the tangent plane, $\vec{v}_o$, $\vec{v}_s$ $\vec{v}_T$ are connected by the following equations ($v = |\vec{v}|$):

$$(1)\quad \tan\varphi_s = \tan\varphi_o + \frac{v_T}{v_o \cos\varphi_o \cos\psi_o}$$

$$(1a)\quad \tan\varphi_o = \tan\varphi_s - \frac{v_T}{v_s \cos\psi_s \cos\varphi_s}$$

$$(2)\quad v_s = v_o\left[1 + 2\left(\frac{v_T}{v_o}\right)\sin\varphi_o \sin\psi_o + \left(\frac{v_T}{v_o}\right)^2\right]^{1/2}, \quad v_T = \omega R \cos B$$

$$(3)\quad v_s \sin\psi_s = v_o \sin\psi_o$$

$\varphi$ is the azimuth of ejection, counted clockwise from y to x, $\psi$ the elevation of ejection measured from the tangent plane on the sphere in S.

The time of flight along the elliptical orbit o for an angular range $2\eta_s$ is given by (Kooy and Uytenbogaart 1946):

$$(4)\quad t_f = \frac{a^{3/2}}{R\sqrt{g_o}}\left[\theta - \epsilon \sin u\right] \qquad \begin{aligned} \theta &= \pi + \eta \\ \theta &= \pi - \eta \end{aligned}$$

$$(4a)\quad \tan\frac{u}{2} = \sqrt{\frac{1-\epsilon}{1+\epsilon}}\,\tan\frac{\theta}{2}$$

$$(5)\quad \epsilon = \frac{\nu_s \cos\psi_s}{g_o R}\sqrt{\nu_s^2 - 2g_o R + \frac{g_o^2 R^2}{\nu_s^2 \cos\psi_s^2}}$$

$$(6)\quad a = \frac{g_o R^2}{\nu_{esc}^2 - \nu_s^2}$$ = the half major axis of the elliptical orbit.

$\nu_{esc} = \sqrt{2g_o R}$ is the escape-velocity on the moon, equal to 2.373 km per sec. Calculations for $t_f$ were based upon a mean radium $R = 1.738 \times 10^6$ m and a $g_o$ of 1.62 m per $sec^2$. (Fielder 1961), the results for selected values of $2\eta_s$ are given in Fig. 3.

Application of the law of cosines and the law of sines in the triangle SMF (Fig. 4) leads to an equation connecting the half range $\eta_s$ and the angle $\psi_s$:

$$(7)\quad \sin\eta_s = \frac{\ell \sin 2\psi_s}{\sqrt{R^2 + \ell^2 - 2R\ell\cos 2\psi_s}}$$

with (7a) $\ell = 2a - R.$

For velocities $\nu_s$ near to the escape velocity, the half major axis a, and therefore $\ell$, becomes very large as compared with R, reducing equation (7) to:

$$(8)\quad \sin\eta_s = \sin 2\psi_s \quad (\frac{R}{\ell} \ll 1)$$

Thus the steepest angle of ejection for an angular range $2\eta_s$ follows to be:

$$(8a)\quad \psi_s\,(max) = 90 - \frac{1}{2}\eta_s .$$

The product $\nu_s \cos\psi_s$ (Fig. 5) therefore has a minimum value for each $2\eta_s$ given by:

$$(9)\quad \nu_s \cos\psi_s = \nu_{esc} \cdot \cos(90 - \frac{1}{2}\eta_s) = \nu_{esc} \cdot \sin\frac{1}{2}\eta_s$$

It never becomes zero except for vertical ejection i.e. $2\eta_s = 0$.

With $\nu_s \approx \nu_{esc}$ the time of flight is approximately

$$(10)\quad t_f = \frac{2\pi}{R\sqrt{g_o}}\, a^{3/2} = 2.84 \cdot 10^{-6}\, a^{3/2} \quad \text{(sec)} \quad [\text{a in meters}]$$

This is of course the time needed to complete the total ellipse from S to S, but the arc below the moon's surface is considerably smaller than the arc covered by the particle. $t_f$ goes continuously towards infinity as $\nu_s$ approaches $\nu_{esc}$.

III. Evidences for a Change in Tycho's Position with Respect to the Axis of Rotation

Fig. 6 shows the position of the rays with Tycho as center, plotted in parallel-projection from a lunar photograph (Kuiper 1960). The moon was considered to be an exact sphere and the fact that the photograph shows the moon in a slightly conical projection was not taken into account. In the vicinity of the crater the long rays are obscured by the very dense and irregular pattern of the short ones, which makes it impossible to trace them without too much uncertainty.

There is some evidence, that Tycho's position with respect to the axis of rotation has changed after the deposition of the rays. The system shows both left- and right-handed curvature with a distinct symmetry, indicating that Tycho once has been near or even on the equator. Ray 2 has an extremely small deviation from a great circle, which is hard to explain on basis of the present position of Tycho with respect to the moon's axis. Being close to the equator, as in Fig. 6, the ray would show almost no curvature, as the deviation $\Delta c$ occurs mainly in the direction of the ray. With Tycho on the equator there is also no difficulty in explaining the loops of ray 7 and 8. As soon as a particle passes over the limb ($2\eta_s > 90°$), it moves--in the projection--towards the source again (Fig. 7). If the time of flight is long enough, the rotation of the moon will cause the particle to fall at the point $P'_2$ in Fig. 7. The summit $P_1$ corresponds to an angular range $2\eta_s$ of 90°. As an additional condition one finds that the great circle c must not cross the ray if all particle orbits have been in the same vertical plane.

As a result Tycho was taken as having been directly on the equator with the center of the crater as the source of the ejected material. Based on these assumptions there are two extreme possibilities for choosing the angular position of the equator:

a) $\varphi_s$ for ray 7 as small as possible, i.e. the great circle tangent to the point nearest to Tycho; $P'_1$ and $P_1$ (Fig. 7) thus give the parallel circle p and the direction of the equator.

b) The second extreme position is given with the equator passing through the innermost point of ray 2.

Although both positions are too extreme--they do not allow any deviation $\Delta\alpha$ in the reference points--their angular distance is only 5.5 degrees. The equator was chosen in the middle of both extreme values, thus having a maximum error of 2.75°. Fig. 8 gives the position of the old equator and the corresponding poles with respect to the lunar coordinate system now in use. The point of intersection lies at 5° West (175° East respectively), the angle of inclination is 72.5°, and the poles have the coordinates: 95 W, 17.5 S; 85 E, 17.5 N. The error for all angles is approximately $\pm$ 3°.

There is no explanation for the drift of the moon's crust with respect to the axis of rotation, but on the earth too, one has many indications for polar shifts in recent geological periods, which are of the same order of magnitude as calculated above (Hapgood 1958).

IV. Period of Revolution; Age of the Tycho-system

Rays 7 and 8 served as a basis for an attempt to determine the period of rotation at the time when Tycho and its system were formed, because their azimuths $\varphi_s$ are the only ones known with small error. Therefore Fig. 9 gives the deviation only along these two rays in detail. However, the assumption that $\varphi_s$ is the same for all ranges $2\eta_s$ in one ray, which was taken as a basis for the determination of $\Delta\alpha$, does not hold exactly. The term

$$\Delta \tan \varphi_o = \frac{\nu T}{\nu_s \cos \phi_o \cos \psi_o} = \frac{\nu T}{\nu_o \cos \psi_o \cos \varphi_o}$$

in equation (1) and (1a) depends upon $2\eta_s$, because of the variations in $\nu_s \cos \psi_s$ ($\nu_o \cos \varphi_o$ respectively Fig. 5). The quantity $\Delta \tan \varphi_o$ decreases with increasing angular range, and if $\varphi_s - \varphi_o$ is about one degree at $2\eta_s = 15°$ the difference is negligibly small for a $2\eta_s \geqq 90°$.

The width of the ray consists of two main components: The initial width "$\delta$" of the particle-beam at the moment of ejection and, in addition to that, ray broadening which occurs during the deposition of the material because of differing orbits (with differences in $t_f$) for the same $2\eta_s$. Therefore the distortion of the ray as a consequence of the variable $\Delta \tan \varphi_o$ will not be obvious as long as the displacement $\varphi_s - \varphi_o = \Delta\varphi$ is smaller than the half angular width of the ray. The ray broadening during the deposition, will then obscure the effect of the differences in the angular displacement. For a total width of 3°, as calculated for the rays 7 and 8 at $2\eta_s = 15°$, $\Delta\varphi$ should not exceed 1 to 1.5 degrees. To allow for the "time dependent" ray broadening $\Delta\varphi$ was taken to be only 1 degree. For ray 8 one gets:

$$\varphi_s \cong \varphi_o^{(90)} = 61.5°;\ \Delta\varphi = 1°\ (\text{at } 2\eta_s = 15°),\ \varphi_s^{(15)} = \varphi_o + 1° = 62.5°$$

and from equation 1a:

$$(\tan 62.5 - \tan 61.5) \cos 62.5 = \nu_\tau / (\nu_s \cos \psi_s) \leqq 3.6.10^{-2}$$

Beginning with a $\tau$ of one day ($\nu_\tau = 0.1264$ km per second) one first has to calculate the time of flight from the measured value of $\Delta\alpha$, which is 4.3° ($2\eta_s = 15°$, Fig. 9). The resulting $t_f = 1032$ sec corresponds to a $\psi_s$ of approximately 54.5° (Fig. 3). From Fig. 5 one finds $\nu_s \cos \psi_s = 0.48$ ($2\eta = 15°; \psi_s = 54.5°$). The resulting value of $\nu_\tau / (\nu_s \cos \psi_s) = 0.26$ is about seven times larger than the limit, which was calculated above. As one finds, all periods smaller than 20 days do not fulfill the basic assumptions. For a $\tau = 20$ days, $t_f$ is 20640 sec, $\psi_s$ close to 85° ($t_f$ at 85° = 17800 sec, $t_f$ at 86.25° $\rightarrow \infty$), and $\nu_s \cos \psi_s = 0.175$. $\nu_\tau / \nu_s \cos \psi_s$ therefore is $3.6.10^{-2}$. This means, that a period of 20 days is the shortest one to fulfill the preceeding assumptions, i.e. it brings $\Delta\varphi$ into the required limit. A similar calculation on ray 7 results in a $\tau$ of 18.4 days.

The next step was to calculate the velocity spectra of both rays, which was done for a $\tau$ of 20 days. The values of $t_f$ resulting from this $\tau$ and the

$\Delta\alpha$ in Fig. 9 indicate, that the angle of ejection $\psi_s$ in each case was close to $\psi_s$ (max) (Equation 8a) (For instance: $\psi_s$ (max) = 86.25° for $2\eta_s = 15°$, $\psi_s$ calculated: >85°). The corresponding major axis based on $t_f$ therefore is given by equation 10 and $\nu_s$ found from equation 6. For $2\eta_s = 15°$, where the errors are largest, the exact value of $\nu_s = 2.05$ km per sec, the approximation yields 2.08 km per sec (ray 8). The velocity spectra in Fig. 10 give $\nu_s$ versus $\psi_s$, which is very close to $\nu_o$ versus $\psi_o$, as $\nu_T = 0.006$ km per sec $\ll \nu_o$. The velocity $\nu_o$ is nearly constant, but it shows a sharp decrease for $\psi_s \geqq 81°$ to 83°. This seems to be similar for all rays, as far as one can judge without knowing the exact value of $\varphi_s$. Small variations in $\nu_s$ for the same $\psi_s$ result in orbits with different major axes and cause the broadening of the particle beam during the deposition. Even for the largest values of 2a the centrifugal force is smaller than $10^{-3}$ m per sec$^2$, which is certainly within the error of $g_o = 1.62$ m per sec$^2$; it was therefore neglected in all calculations.

Finally one comes to the conclusion: The material was ejected with velocities close to the escape velocity. In this case, the range $2\eta_s$ is given only by the angle of ejection according to equation 8a and the time of flight by the velocity (Equation 6 and 10) independent of $\psi_s$. This fact avoids a complex velocity-structure of the particle beam and a mathematical dependence of $\nu_s$ on $\psi_s$.

On the basis of Jeffreys' theory (1952) one can calculate the time which elapsed since the formation of the Tycho system; the result is $2.6 \times 10^9$ years (for a $\tau$ of 20 days), making Tycho comparable in age with similar structures on the earth. The Vredefort ring structure in South Africa, for instance, dates from the late Precambrian (Daly 1947), a geological period ending about $0.5 \times 10^9$ years ago (Wilson 1954).

Figure Captions

Fig. 1: Orbit of a particle on a rotating sphere. (c, $c_t$ = great circles, $\varphi_s$ = azimuth of ejection, $\vec{\nu}_s$ = initial velocity in the orbit o).

Fig. 2: $\nu_s$, $\nu_o$ and $\nu_\tau$ in the coordinate-system used for the derivation of equations 1, 1a, 2, 3.

Fig. 3: Time of flight $t_f$ versus the angle of ejection for a selected number of angular ranges. ($R = 1.738.10^6$ m, $g_o = 1.62$ m per $sec^2$).

Fig. 4: Elliptical orbit of a particle in a central symmetric gravity field. $\eta$ = half angular-range on the moon's surface. (Equations 4 and 7).

Fig. 5: $\nu \cos\psi$ as a function of the angle of ejection. All curves converge in the point $\nu \cos\psi = 1.68$ km per sec for $\psi = 0$ and $\nu$ equal to the circular velocity on the moon's surface.

Fig. 6: The ray-system of Tycho in parallel projection, e' = old equator. (dashed lines indicate extreme positions). Ray 2 extends towards Mare Serenitatis (dotted line).

Fig. 7: Formation of a loop in a ray extending in the direction of rotation.

Fig. 8: Position of the old poles and the old equator e' in the lunar coordinate-system.

Fig. 9: Deviation $\Delta\alpha$ as a function of $2\eta_s$. The dashed lines indicate the field of $\Delta\alpha$ for all rays except 7 and 8.

Fig.10: Velocity-spectrum of the rays number 8 and 7 in polar coordinates.

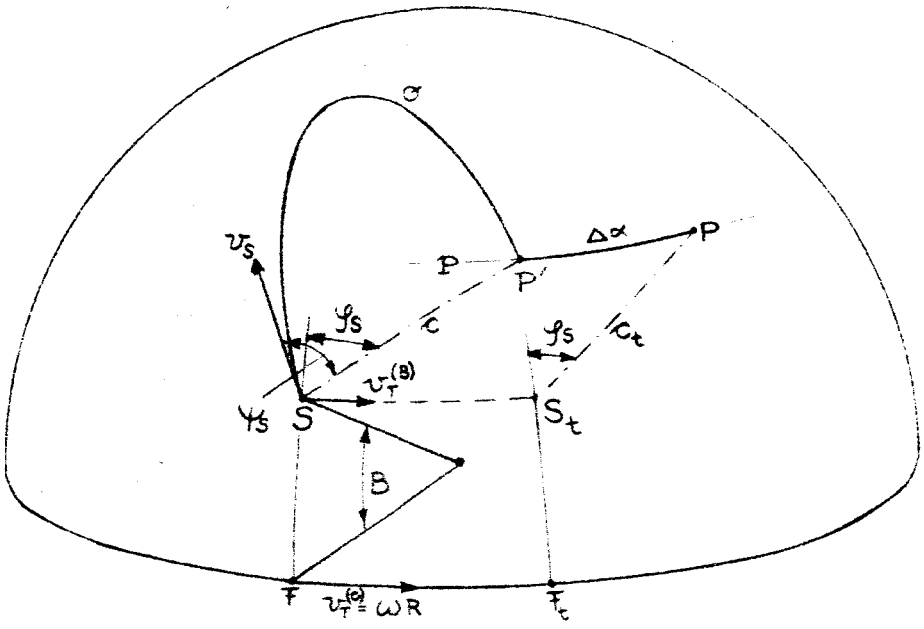


Fig. 1

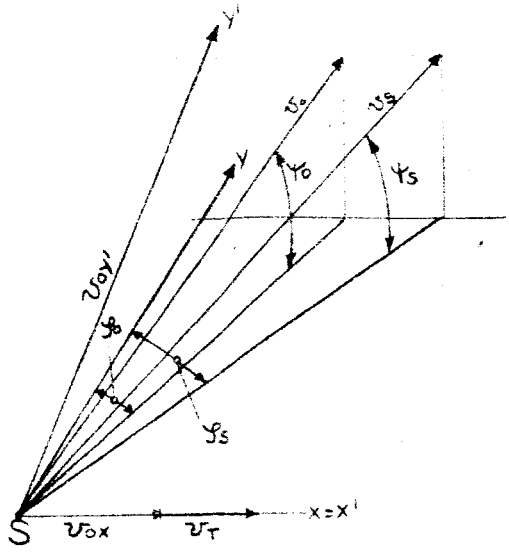


Fig. 2



Carl Clark

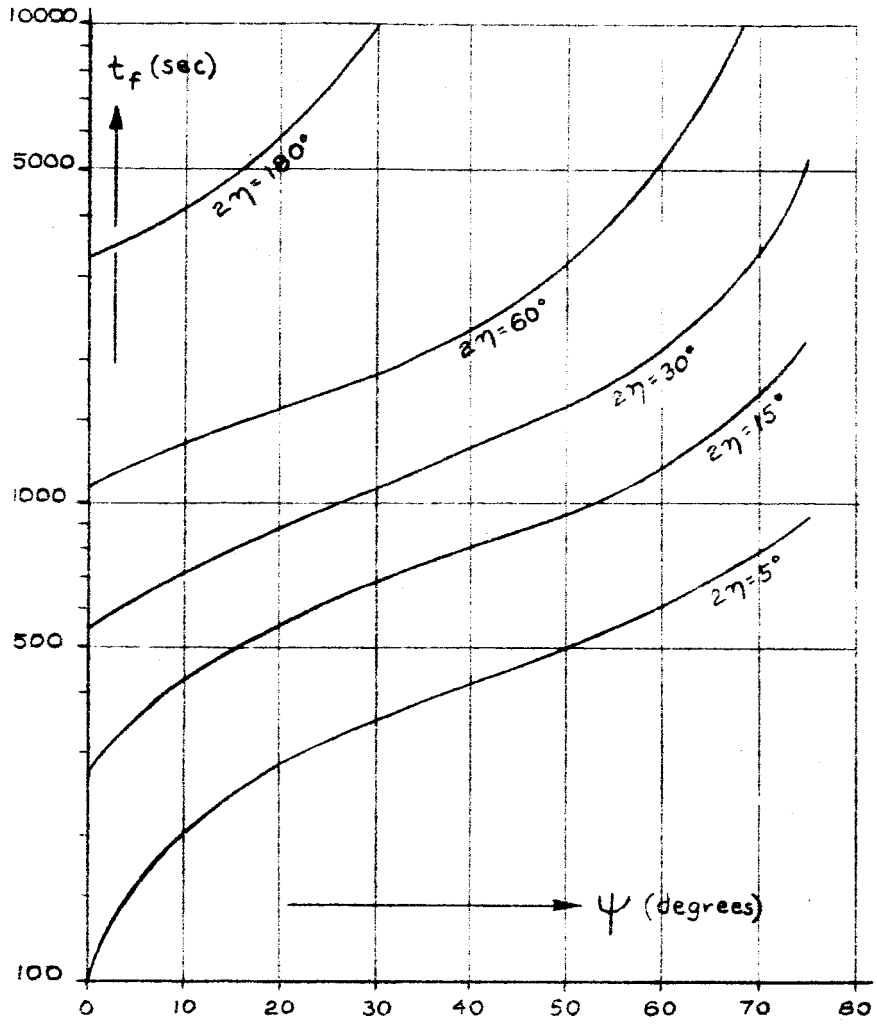
10000
5000
1000
500
100
$t_f$ (sec)
$2\eta = 120°$
$2\eta = 60°$
$2\eta = 30°$
$2\eta = 15°$
$2\eta = 5°$
$\psi$ (degrees)
0
10
20
30
40
50
60
70
80

Fig. 3

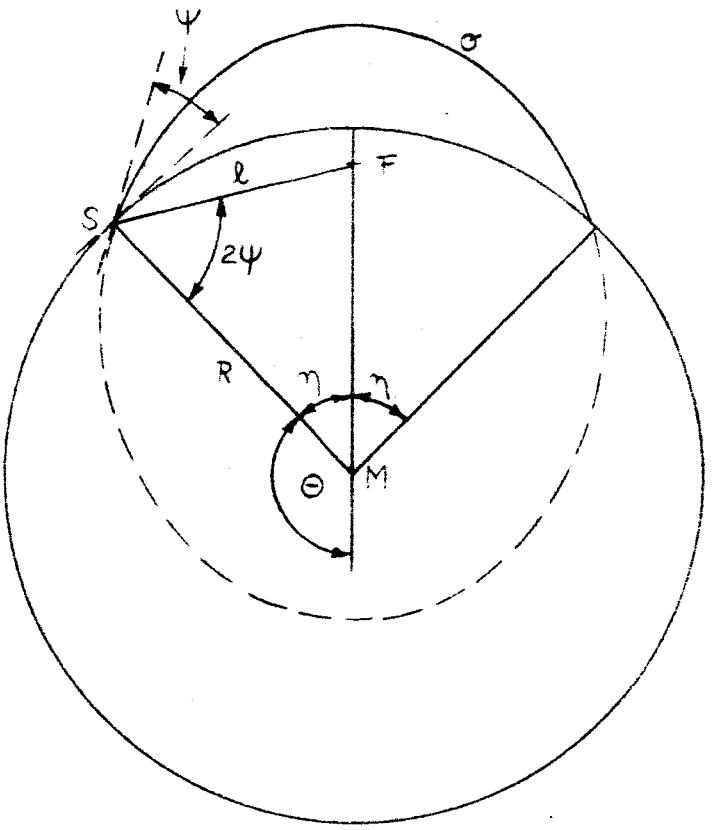
Ψ
σ
ℓ
F
S
2Ψ
R
η
η
Θ
M

Fig. 4

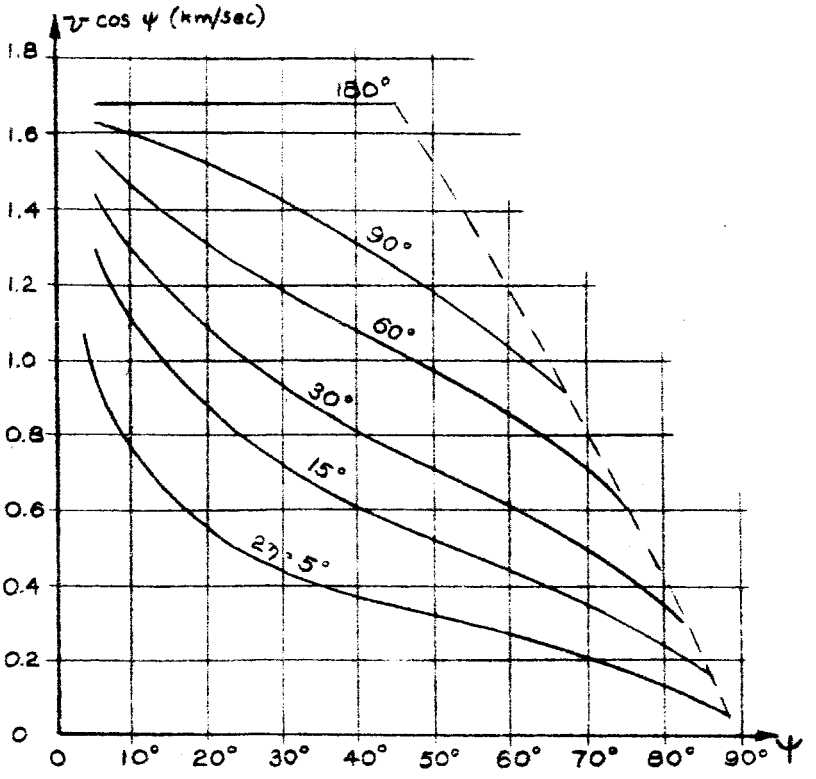
v cos ψ (km/sec)
1.8
1.6
1.4
1.2
1.0
0.8
0.6
0.4
0.2
0
180°
90°
60°
30°
15°
22.5°
0
10°
20°
30°
40°
50°
60°
70°
80°
90°
ψ

Fig. 5

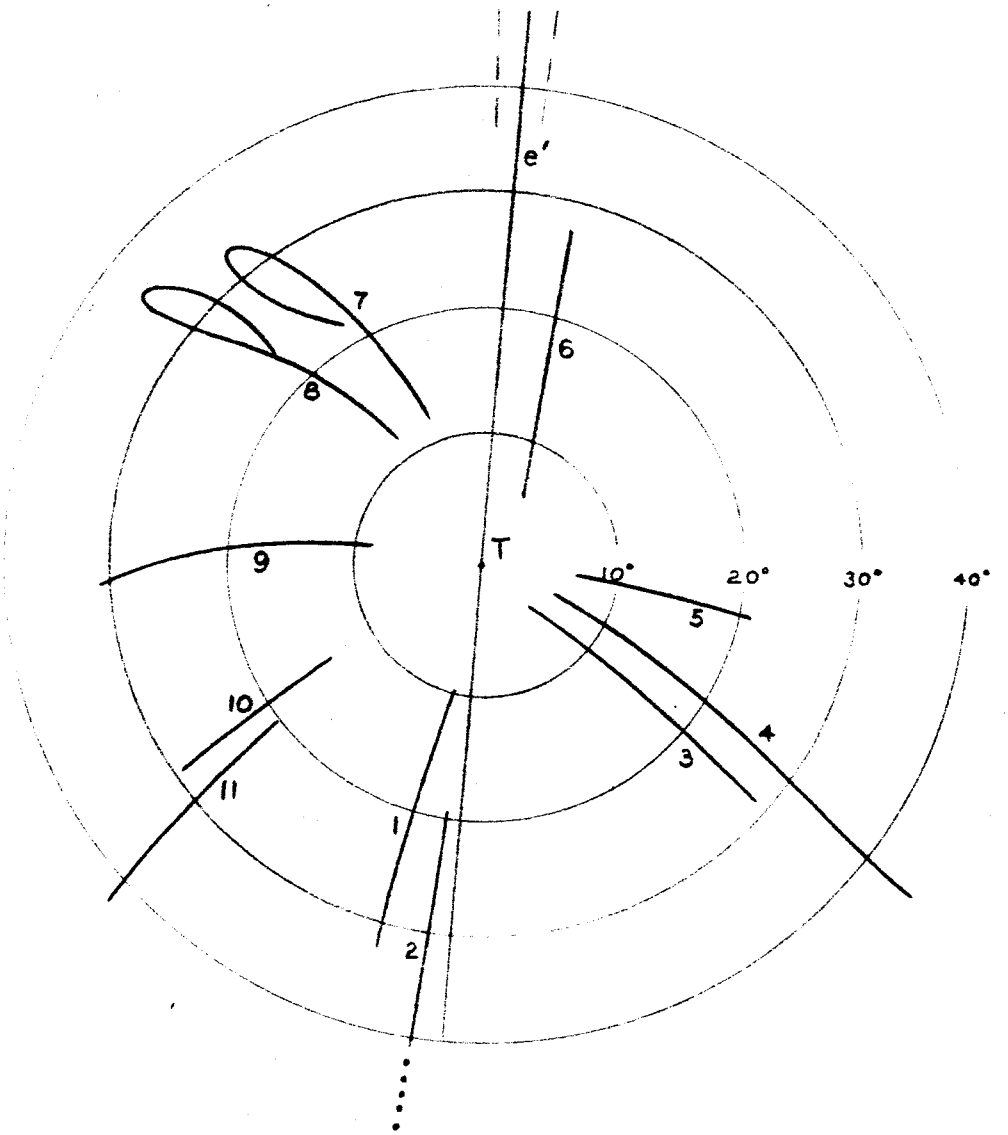


Fig. 6

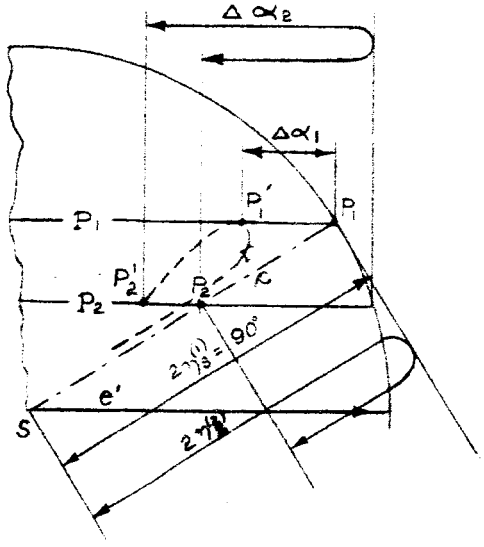


Fig. 7

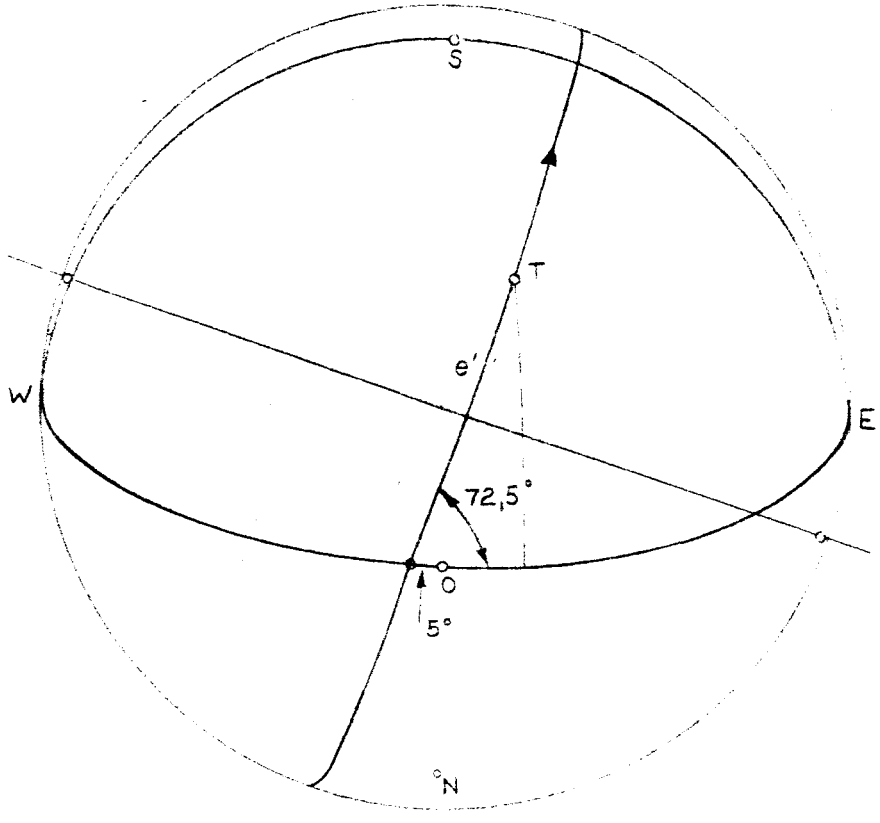


Fig. 8

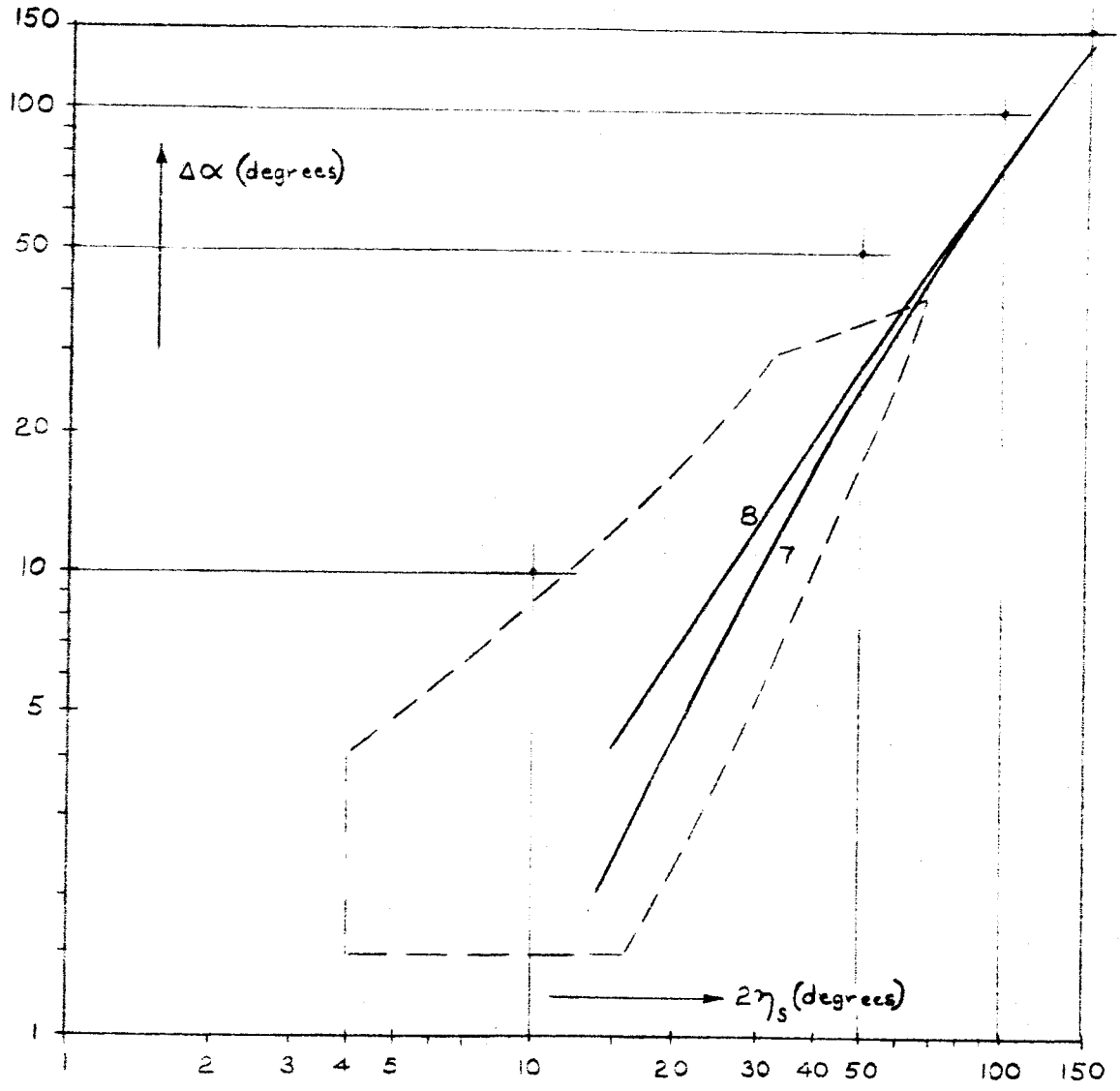
150
100
50
20
10
5
1
Δα (degrees)
8
7
2η_s (degrees)
1
2
3
4
5
10
20
30
40
50
100
150

Fig. 9

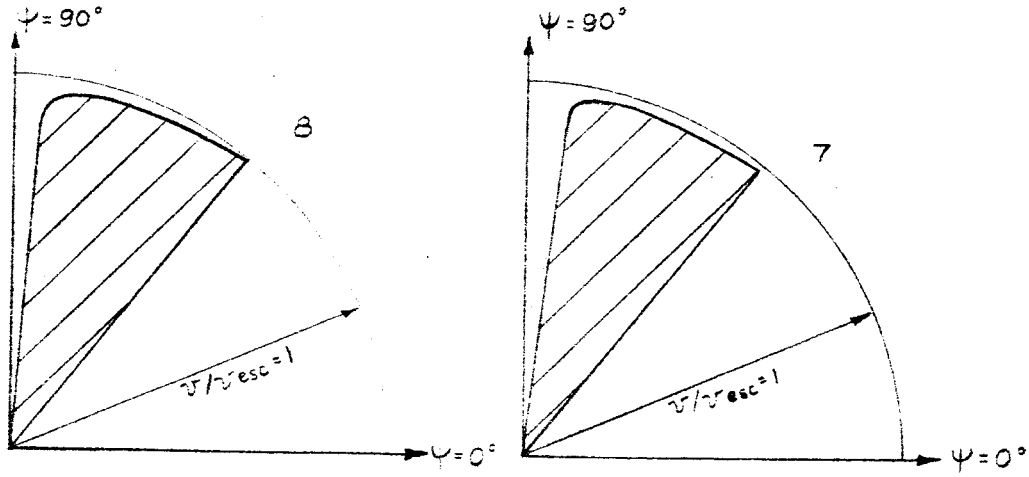


Fig. 10

References

1. Daly A. R., Journ. of Geol., Vol. 55, 125 - 145, (1947).
2. Fielder G., Structure of the Moon's Surface, Pergamon Press, 1st Edit., (1961).
3. Giamboni L. A., Astrophys. Journ., Vol. 130, 324 - 335, (1959).
4. Hapgood C. H., Earth's Shifting Crust, Pantheon Book, 1st Edit. (1958).
5. Jeffreys H., The Earth, Cambridge Univ. Press, 3rd Edit. (1952).
6. Kooy J. M. J., Uytenbogaart J. W. H., Ballistics of the Future, 1st Edit., McGraw-Hill Book Co., (1946).
7. Kuiper G. P., Photographic Lunar Atlas, 1st Edit., Univ. of Chicago Press (1960).
8. Wilson J. T., in Kuiper G. P (Editor), The Earth as a Planet, 1st Edit., Univ. of Chicago Press, (1954).
9. Wright F. E., et al., in Middlehurst B. M., Kuiper G. P. (Editors) The Moon, Meteorites and Comets, 1st Edit., Univ. of Chicago Press, (1963).

BIOGRAPHY

Martin Sedlacek

Personal:

Born - May 1, 1936. Wiener Neustadt, Austria (Austrian Citizen)

Education:

Ph.D. (Physics), University of Wien, 1961.
Post-doctoral study, University of Colorado, NASA Fellowship, September 1963 to present

Positions and Technical Experience:

Scientific Aid, First Physics Inst., Univ. of Wien, Austria, 1959-1961
Assistant Prof., First Physics Inst., Univ. of Wien, Austria, August 1961

Publications:

"Gammaspektrometrie von Staubproben" Staub 22., 87-90, (1962)
"Uber Messungen der langlebigen Radioaktivitat" Mitteil. der Osterr. San. Verwaltung 63., 3-16, (1962) (Co-author)
"Sizing the Fall-Out at Vienna" Nature 195, No. 4845, 986-987 (1962) (Co-author)
"Korngrossenverteilung und Haufigkeit des langlebig radioaktiven Aerosols in der bodennahen Atmosphare" Acta Physica Austriaca 16., 296-303, (1963) (Co-author)
"Fallout-Untersuchungen im Raum von Wien in der Zeit vom 1. September 1961 bis 30. Juni 1963" Staub 23., 407-412 (1963) (Co-author)